A&A 567, A54 (2014)
DOI: 10.1051/0004-6361/201323313

Astronomy & Astrophysics

Diversity of planetary systems in low-mass disks

Terrestrial-type planet formation and water delivery

M. P. Ronco and G. C. de Elía

Facultad de Ciencias Astronómicas y Geofísicas, Universidad Nacional de La Plata and Instituto de Astrofísica de La Plata, CCT La Plata-CONICET-UNLP, Paseo del Bosque S/N, 1900 La Plata, Argentina
e-mail: mpronco@fcaglp.unlp.edu.ar

Received 20 December 2013 / Accepted 5 May 2014

ABSTRACT

Context. Several studies, observational and theoretical, suggest that planetary systems with only rocky planets are the most common in the Universe.
Aims. We study the diversity of planetary systems that might form around Sun-like stars in low-mass disks without gas-giant planets. We focus especially on the formation process of terrestrial planets in the habitable zone (HZ) and analyze their water contents with the goal to determine systems of astrobiological interest. In addition, we study the formation of planets on wide orbits because they can be detected with the microlensing technique.
Methods. N-body simulations of high resolution were developed for a wide range of surface density profiles. A bimodal distribution of planetesimals and planetary embryos with different physical and orbital configurations was used to simulate the planetary accretion process. The surface density profile combines a power law for the inside of the disk of the form $r^{-\gamma}$, with an exponential decay to the outside. We performed simulations adopting a disk of 0.03 $M_\odot$ and values of $\gamma = 0.5$, 1 and 1.5.
Results. All our simulations form planets in the HZ with different masses and final water contents depending on the three different profiles. For $\gamma = 0.5$, our simulations produce three planets in the HZ with masses ranging from 0.03 $M_\oplus$ to 0.1 $M_\oplus$ and water contents between 0.2 and 16 Earth oceans (1 Earth ocean = $2.8 \times 10^{-4} M_\oplus$). For $\gamma = 1$, three planets form in the HZ with masses between 0.18 $M_\oplus$ and 0.52 $M_\oplus$ and water contents from 34 to 167 Earth oceans. Finally, for $\gamma = 1.5$, we find four planets in the HZ with masses ranging from 0.66 $M_\oplus$ to 2.21 $M_\oplus$ and water contents between 192 and 2326 Earth oceans. This profile shows distinctive results because it is the only one of those studied here that leads to the formation of *water worlds*.
Conclusions. Since planetary systems with $\gamma = 1$ and 1.5 present planets in the HZ with suitable masses to retain a long-lived atmosphere and to maintain plate tectonics, they seem to be the most promising candidates to be potentially habitable. Particularly, these systems form Earths and Super-Earths of at least 3 $M_\oplus$ around the snow line, which can be discovered by the microlensing technique.

Key words. astrobiology – methods: numerical – protoplanetary disks

1. Introduction

The accretion process that leads to the formation of terrestrial planets is strongly dependent on the mass distribution in the system and on the presence of gas-giant planets. Therefore, it is necessary to consider protoplanetary disks with different surface density profiles as well as several physical and orbital parameters for the gas giants to analyze the diversity of planetary systems that might form around solar-type stars.

During the past years, several observational works have suggested that the planetary systems consisting only of rocky planets are the most common in the Universe. In fact, using precise radial velocity measurements from the Keck planet search, Cumming et al. (2008) inferred that 17%–19% of the solar-type stars have giant planets with masses $M > 100\ M_\oplus$ within 20 AU. More recently, Mayor & Queloz (2012) analyzed the results of an eight-year survey carried out at the La Silla Observatory with the HARPS spectrograph and suggested that about 14% of the solar-type stars have planets with masses $M > 50\ M_\oplus$ within 5 AU. On the other hand, many theoretical works complement these results. For example, Mordasini et al. (2009) developed a great number of planet population synthesis calculations of solar-like stars within the framework of the core-accretion scenario. From this theoretical study, these authors indicated that the occurrence rate of planets with masses $M > 100\ M_\oplus$ is 14.3%, which agrees with that obtained by Cumming et al. (2008). More recently, Miguel et al. (2011) developed a semi-analytical code for computing the planetary system formation, based on the core instability model for the gas accretion of the embryos and the oligarchic growth regime for the accretion of solid cores. The most important result obtained by these authors suggests that planetary systems with only small rocky planets represent probably the vast majority in the Universe.

The standard model of solar nebula (MSN) developed by Weidenschilling (1977) and Hayashi (1981) predicts that the surface densities of dust materials and gases vary approximately as $r^{-1.5}$, where r is the distance from the Sun. This model is constructed by adding the solar complement of light elements to each planet and then by distributing this augmented mass uniformly across an annulus around the location of each planet. Davis (2005) reanalyzed the MSN nebula and predicted that the surface density follows a decay rate of $r^{-0.5}$ in the inner region and a subsequent exponential decay. Later, Desch (2007) adopted the starting positions of the planets in the Nice model (Tsiganis et al. 2005) and suggested that the surface density of the solar nebula varies approximately as $r^{-2.2}$. On the other

hand, detailed models of structure and evolution of protoplanetary disks (Dullemond et al. 2007; Garaud & Lin 2007) suggest that the surface density falls off with radius much less steeply (as r^{-1}) than that assumed for the MSN. More recently, Andrews et al. (2009, 2010) analyzed protoplanetary disk structures in the Ophiuchus star-forming region. They inferred that the surface density profile follows a power law in the inner disk of the form $r^{-\gamma}$ and an exponential taper at large radii, where γ ranges from 0.4 to 1.1 and shows a median value of 0.9.

Several authors have tried to build a minimum-mass extrasolar nebula (MMEN) using observational data of exoplanets. On the one hand, Kuchner (2004) used 11 systems with Jupiter-mass planets detected by radial velocity to construct an MMEN. On the other hand, Chiang & Laughlin (2013) used *Kepler* data of planetary candidates with radii $R < 5R$ to build an MMEN. Both analyses produced steep density profiles. In fact, Kuchner (2004) predicted that the surface density varies as r^{-2} for the gas giants, while Chiang & Laughlin (2013) suggested that the surface density follows a decay rate of $r^{-1.6}$ for the super-Earths. Recently, Raymond & Cossou (2014) suggested that it is inconsistent to assume a universal disk profile. In fact, these authors predicted that the minimum-mass disks calculated from multiple-planet systems show a wide range of surface density slopes.

Several previous studies have analyzed the effects of the surface density profile on the terrestrial planet formation in a wide range of scenarios. On the one hand, Chambers & Cassen (2002) and Raymond et al. (2005) examined the process of planetary accretion in disks with varying surface density profiles in presence of giant planets. On the other hand, Kokubo et al. (2006) investigated the final assemblage of terrestrial planets from different surface density profiles considering gas-free cases without gas giants. While these authors assumed disks with different masses, they only included planetary embryos (no planetesimals) in a narrow radial range of the system between 0.5 AU–1.5 AU. Raymond et al. (2007b) simulated the terrestrial planet formation without gas giants for a wide range of stellar masses. For Sun-like stars, they developed simulations in a wider radial range (from 0.5 AU to 4 AU) than that assumed by Kokubo et al. (2006). However, like Kokubo et al. (2006), Raymond et al. (2007b) did not examine the effects of a planetesimal population in their simulations.

Here, we show results of N-body simulations aimed at analyzing the process of formation of terrestrial planets and water delivery in absence of gas giants. It is important to highlight that these are high-resolution simulations that include planetary embryos and planetesimals. In particular, our work focuses on low-mass protoplanetary disks for a wide range of surface density profiles. This study is motivated by an interesting result obtained by Miguel et al. (2011), which indicates that a planetary system composed of only rocky planets is the most common outcome obtained from a low-mass disk (namely, $\lesssim 0.03\ M_{\odot}$) for different surface density profiles. The most important goal of the present work is to analyze the potential habitability of the terrestrial planets formed in our simulations. From this, we will be able to determine if the planetary systems under consideration are targets of astrobiological interest.

Basically, the permanent presence of liquid water on the surface of a planet is the main condition required for habitability. However, the existence of liquid water is a necessary but not sufficient condition for planetary habitability. In fact, organic material, the preservation of a suitable atmosphere, a magnetic field, and tectonic activity represent other relevant conditions for the habitability of a planet. The N-body simulations presented here allow us to describe the dynamical evolution and the accretion history of a planetary system. From this, it is possible to analyze the water delivery to the resulting planets, primarily to those formed in the habitable zone (HZ), which is defined as the circumstellar region inside which a planet can retain liquid water on its surface. Therefore the criteria adopted in the present paper to determine the potential habitability of a planet are based on its location in the system and its final water content.

This paper is therefore structured as follows: in Sect. 2, we present the main properties of the protoplanetary disks used in our simulations. Then, we discuss the main characteristics of the N-body code and outline our choice of initial conditions in Sect. 3. In Sect. 4, we present the results of all simulations. Finally, we discuss these results within the framework of the current knowledge of planetary systems and present our conclusions in Sect. 6.

2. Protoplanetary disk: properties

Here we describe the model of the protoplanetary disk and then define the parameters we need to develop our simulations.

The surface density profile is one of the most relevant parameters to determine the distribution of material in the disk. In this model, the gas surface density profile that represents the structure of the protoplanetary disk is specifically given by

$$\Sigma_{\rm g}(r) = \Sigma_{\rm g}^0 \left(\frac{r}{r_{\rm c}}\right)^{-\gamma} {\rm e}^{-\left(\frac{r}{r_{\rm c}}\right)^{2-\gamma}}, \tag{1}$$

where $\Sigma_{\rm g}^0$ is a normalization constant, $r_{\rm c}$ a characteristic radius, and γ the exponent that represents the surface density gradient. By integrating Eq. (1) over the total area of the disk, $\Sigma_{\rm g}^0$ can be expressed by

$$\Sigma_{\rm g}^0 = (2-\gamma)\frac{M_{\rm d}}{2\pi R_{\rm c}^2}. \tag{2}$$

This surface density profile combines a power law for the inside of the disk, with an exponential decay to the outside, and is based on the similarity solutions of the surface density of a thin Keplerian disk subject to the gravity of a point mass ($M_\star$) central star (Lynden-Bell & Pringle 1974; Hartmann et al. 1998).

Analogously, the solid surface density profile $\Sigma_{\rm s}(r)$ is represented by

$$\Sigma_{\rm s}(r) = \Sigma_{\rm s}^0 \eta_{\rm ice} \left(\frac{r}{r_{\rm c}}\right)^{-\gamma} {\rm e}^{-\left(\frac{r}{r_{\rm c}}\right)^{2-\gamma}}, \tag{3}$$

where $\eta_{\rm ice}$ represents an increase in the amount of solid material due to the condensation of water beyond the snow line. According to the MSN of Hayashi (1981), $\eta_{\rm ice}$ is 1/4 inside and 1 outside the snow line, which is located at 2.7 AU[1].

After deriving the value of $\Sigma_{\rm g}^0$, the relation between both profiles allows us to know the abundance of heavy elements, which is given by

$$\left(\frac{\Sigma_{\rm s}^0}{\Sigma_{\rm g}^0}\right)_\star = \left(\frac{\Sigma_{\rm s}^0}{\Sigma_{\rm g}^0}\right)_\odot 10^{[{\rm Fe/H}]} = z_0 10^{[{\rm Fe/H}]}, \tag{4}$$

where z_0 is the primordial abundance of heavy elements in the Sun and [Fe/H] the metallicity.

[1] Although we used the classic model of Hayashi (1981), is worth noting that Lodders (2003) found a much lower value for the increase in the amount of solids due to water condensation beyond the snow line. This value corresponds to a factor of 2 instead of 4.

After the model is presented, we need to quantify some parameters for the disk. We assumed that the central star of the protoplanetary disk is a solar metallicity star, [Fe/H] = 0, with $M_\star = 1\ M_\odot$. Then, $\Sigma_s^0 = z_0 \Sigma_g^0$ where $z_0 = 0.0149$ (Lodders 2003). We considered a low-mass disk with $M_d = 0.03\ M_\odot$ because this value for the mass guarantes that no giant planets are formed (Miguel et al. 2011).

The exponent γ is another relevant parameter for this model because it establishes an important characteristic of the simulation scenario: the higher the exponent, the more massive the disk in the inner part of it. In this work we explore three different values for the exponent: $\gamma = 0.5$, 1 and 1.5. These values represent disks in a range from rather flat ones ($\gamma = 0.5$) where the density of gas and solids is well distributed and there are no preferential areas for the accumulation of gas and solids, to steeper profiles ($\gamma = 1.5$) with an accumulation of gas and solids in the inner part of the disk and around the snow line. Finally, for the characteristic radius we adopted $r_c = 50$ AU, which represents a characteristic value of the different disk observations studied by Andrews et al. (2010).

For the water content in the disk, we assumed that the protoplanetary disk presents a radial compositional gradient. Then we adopted an initial distribution of water similar to that used by Raymond et al. (2004, 2006) and Mandell et al. (2007), which was based on the one predicted by Abe et al. (2000). Thus, the water content by mass $W(r)$ assumed as a function of the radial distance r is given by

$$W(r) = \begin{cases} 0.001\%, & r < 2 \text{ AU} \\ 0.1\%, & 2 \text{ AU} < r < 2.5 \text{ AU} \\ 5\%, & 2.5 \text{ AU} < r < 2.7 \text{ AU} \\ 50\%, & r > 2.7 \text{ AU}. \end{cases}$$

We assigned this water distribution to each body in our simulations, based on its starting location. In particular, the model does not consider water loss during impacts, and therefore the water content represents an upper limit. Because this distribution is based on information about the solar system, it is yet unknown whether this is representative of the vast diversity of planetary systems in the Universe. However, we adopted it to study the water content and hence, the potential habitability of the resulting terrestrial planets.

3. *N*-body method: characteristics and initial conditions

The initial time for our simulations represents the epoch in which the gas of the disk has already dissipated[2].

The numerical code used in our N-body simulations is the MERCURY code developed by Chambers (1999). We particularly adopted the hybrid integrator, which uses a second-order mixed variable symplectic algorithm to treat the interaction between objects with separations greater than 3 Hill radii, and a Burlisch-Stoer method for resolving closer encounters. To avoid any numerical error for small-perihelion orbits, we used a non-realistic size for the Sun radius of 0.1 AU (Raymond et al. 2009).

Since our main goal is to form planetary systems with terrestrial planets, we focused on the inner part of the protoplanetary disk, between 0.5 AU and 5 AU. The solid component of the disk presents a bimodal distribution formed by protoplanetary embryos and planetesimals. We used 1000 planetesimals in each simulation. Then, the number of protoplanetary embryos depends on each density profile. Collisions between both components were treated as inelastic mergers that conserve mass and water content. Since N-body simulations are very costly numerically and to reduce CPU time, the model considers gravitational interactions between embryos and planetesimals, but not between planetesimals (Raymond et al. 2006). It is important to emphasize that these N-body high-resolution simulations allow us to describe in detail the dynamical processes involved during the formation and post evolution stages.

With the total mass of the disk, $M_d = 0.03\ M_\odot$, we calculated the mass of solids in the study region and obtained the solid mass before and after the snow line for each profile. For disks with $\gamma = 0.5$ the total mass of solids is 3.21 $M_\oplus$. Disks with $\gamma = 1$ present a total mass of solids of 7.92 $M_\oplus$ and finally, disks with $\gamma = 1.5$ have 13.66 $M_\oplus$. We then distributed the solid mass in accordance with various planetary accretion studies such as Kokubo & Ida (1998): each component, embryos and planetesimals, have half the total mass in the study region. To distinguish both kinds of bodies, the mass adopted for the planetesimals is approximately an order of magnitude lower than those associated with protoplanetary embryos. This is considered both for the *inner zone*, between 0.5 AU and the snow line, and for the *outer zone*, between the snow line and 5 AU.

Since terrestrial planets in our solar system might have formed in 100 Myr–200 Myr (Touboul et al. 2007; Dauphas & Pourmand 2011), we integrated each simulation for at least 200 Myr. To compute the inner orbit with enough precision we used a six day time step. In addition, each simulation conserved energy to at least one part in 10^3.

To begin our simulations with the MERCURY code, we needed to specify some important initial physical and orbital parameters. For disks with $\gamma = 0.5$ we used 24 embryos, 13 in the inner zone with masses of 0.02 $M_\oplus$ and 11 in the outer zone with masses of 0.13 $M_\oplus$. Planetesimals present masses of $3.87 \times 10^{-4}\ M_\oplus$ and $3.09 \times 10^{-3}\ M_\oplus$ in the inner and outer zone, respectively. For $\gamma = 1$ we placed 30 embryos in the disk, 20 in the inner zone with masses of 0.04 $M_\oplus$, and 10 in the outer zone with masses of 0.32 $M_\oplus$. For this density profile, planetesimals present masses of $1.18 \times 10^{-3}\ M_\oplus$ and $9.49 \times 10^{-3}\ M_\oplus$ in the inner and outer zone, respectively. Finally, disks with $\gamma = 1.5$ present 45 embryos, 35 in the inner zone with masses of 0.06 $M_\oplus$, and 10 in the outer zone with masses of 0.47 $M_\oplus$. Planetesimals in these protoplanetary disks have masses of $2.68 \times 10^{-3}\ M_\oplus$ and 0.021 $M_\oplus$ in the inner and outer zone, respectively. As we have mentioned, we used 1000 planetesimals in each simulation, which were distributed between 0.5 AU and 5 AU, to efficiently model the effects of the dynamical friction. For any disk, physical densities of all planetesimals and protoplanetary embryos were assumed to be 3 g cm^{-3} or 1.5 g cm^{-3} depending on whether they were initially located in the inner or outer zone.

The orbital parameters, such as initial eccentricities and inclinations, take random values lower than 0.02 and 0.5°, respectively, both for embryos and planetesimals. In the same way, we adopted random values for the argument of pericenter ω, longitude of ascending node Ω and the mean anomaly M between 0°

[2] We study the processes of planetary formation considering gas-free cases. Thus, we do not model the effects of gas on the planetesimals and planetary embryos of our systems. In particular, the type I migration (Ward 1997), which leads to the orbital decay of embryos and planet-sized bodies through tidal interaction with the gaseous disk, could play a significant role in the evolution of these planetary systems. However, many quantitative aspects of the type I migration are still uncertain and therefore, we decided to neglect its effects here. A detailed analysis of the impact of the type I migration on the planetary systems of our simulations will be developed in a future study.

and 360°. Finally, the semimayor-axis of embryos and planetesimals were generated using the acceptance-rejection method developed by Jonh von Newmann. This technique indicates that if a number a is selected randomly from the domain of a function f, and another number f^* is given at random from the range of such function, the condition $f^* \leq f(a)$ will generate a distribution for a whose density is $f(a)\mathrm{d}a$. In our case, for each density profile under consideration, the f function is represented by

$$f(a) = \frac{2\pi a \Sigma_s(a)}{M}, \quad (5)$$

where M represents the total mass of solids in the study region and $\Sigma_s(a)$ is the solid density profile that we are using. Thus, the a values obtained from this function are accepted as initial conditions for the semimayor-axis of embryos and planetesimals.

4. Results

In this section we present results of the N-body simulations for the formation of terrestrial planets in low-mass disks for different density profiles.

Given the stochastic nature of the accretion process, we performed three simulations for each value of γ with different random number seeds. Although the data analysis takes into account all the simulations per density profile, here we show graphics of the most representative simulation.

The general purpose of this work is to analyze the diversity of planetary systems that we can perform with the N-body simulations. From this, a particular goal is to determine whether these terrestrial planets in the HZ are potentially habitable.

Here we define the HZ for a solar-type star between 0.8 AU and 1.5 AU in agreement with Kasting et al. (1993) and Selsis et al. (2007). However, the evolution of Earth-like planets is a very complex process, and locating a planet in the HZ does not guarantee that there may be developed life. For example, planets with very eccentric orbits may pass most of their periods outside the HZ, not allowing long times of permanent liquid water on their surfaces. To avoid this problem we considered that a planet is in the HZ and can hold liquid water if it has a perihelion $q \geq 0.8$ AU and a aphelion $Q \leq 1.5$ AU (de Elía et al. 2013). These criteria allowed us to distinguish potentially habitable planets.

We considered the water contents to be significant when they are similar to that of Earth. The total amount of water on Earth is still uncertain because the mass of water in the actual mantle is only poor known as yet. While the mass of water on the Earth surface is 2.8×10^{-4} $M_\oplus$ (1 Earth ocean) the mass of water in the Earth mantle is estimated to be between 0.8×10^{-4} $M_\oplus$ and 8×10^{-4} $M_\oplus$ (Lécuyer & Gillet 1998). On the other hand, Marty (2012) suggested that the current water content in the Earth mantle is approximately 2×10^{-3} $M_\oplus$. According to these studies the present-day water content on Earth should be ~0.1% to 0.2% by mass. However, Earth is expected to have had a higher amount of water in the early stages of its formation, which was lost during the process of the core-accretion and by consecutive impacts. In particular, because we considered inelastic collisions in our N-body simulations, the mass and water content are conserved and therefore, the final water contents in the formed planets represent upper limits.

4.1. Simulations with $\gamma = 0.5$

For this density profile we integrated three different simulations for 250 Myr[3].

[3] For this profile we did not prolong the simulations beyond 250 Myr because the CPU time required is very high.

In general terms, the most important characteristics of the systems can be described as follows: the entire study region, from 0.5 AU to 5 AU, contains between six and seven planets at the end of the simulation, with a total mass ranging between 1.5 $M_\oplus$ and 1.6 $M_\oplus$. The mass of each planet is between 0.03 $M_\oplus$ and 0.57 $M_\oplus$. All simulations form planets in the HZ, and they seem to be very small. Their masses range from 0.03 $M_\oplus$ to 0.1 $M_\oplus$ and their water contents from 0.06% to 5.37% of the total mass, which represents from 0.2 to ~6 Earth oceans.

In particular, Fig. 1 shows six snapshots in time of the semimayor-axis eccentricity plane of the evolution of simulation S3, which we consider to be the most representative. At the beginning of the simulation, both embryos and planetesimals are quickly exited. For embryos this excitation is due to their own mutual gravitational perturbations, but because planetesimals are not self-interacting bodies, their excitation is due to perturbations from embryos. In time, the eccentricities of embryos and planetesimals increase until their orbits intersect each other and accretion collisions occur. Then, embryos grow by accretion of other embryos and planetesimals, and there are fewer bodies. By the end of the simulation just a few planets remain in the study region, and the system presents the innermost planet located at 0.72 AU, which has a mass of 0.06 $M_\oplus$, a planet located in the HZ with 0.03 $M_\oplus$, and the most massive planet placed at 2.87 AU with 0.48 $M_\oplus$. The rest of the simulations present similar results.

Figure 1 also reveals the importance of the dynamical friction from the beginning of the simulation. This dissipative force dampens the eccentricities and inclinations of the large planetary embryos embedded in a sea of planetesimals. In particular, Fig. 2 shows the evolution in time of the eccentricities and inclinations of the most and least massive planet of the S3 simulation. The least massive planet reaches highest values of eccentricity and inclination of 0.35 and 13°, while the most massive planet does not exceed values of eccentricity and inclination of 0.12 and 3.15°. Therefore it is clear that planetesimals are fundamental to describe this phenomenon. The three different simulations show similar results for the dynamical friction effects.

After 250 Myr of evolution, many embryos and planetesimals were removed from the disk. The percentage of planetary embryos and planetesimals that still remain in the study region, between 0.5 AU and 5 AU, is 29% and 46%, respectively. These values represent 1.52 $M_\oplus$ and 0.59 $M_\oplus$. However, the last amount of mass in planetesimals only represents 18% of the total initial mass in this region. Thus, we assume that this remaining mass in planetesimals will not modify the final planetary system significantly. In addition, the remaining mass in planetesimals in the disk at 200 Myr is 0.67 $M_\oplus$, which represents 20% of the initial mass. Hence, there are no significant differences after 50 Myr more of evolution.

Although the orbits of the second and the third planets in S3 cross each other, which means that they could collide and form a single planet in the HZ if we extended the simulations, the final mass of it would not exceed 0.07 $M_\oplus$. In Sect. 5, we discuss the requirements for a planet to be potencially habitable by including its final mass.

The most important mass-removal mechanism both for embryos and planetesimals is mass accretion. With this density profile no embryo collides with the central star, and none of them is ejected from the system. Only 2.2% of the planetesimals collide with the central star and 0.1% (only one planetesimal) is ejected from the disk. These results are consistent with this scenario because it is the least massive profile in the inner zone of the disk.

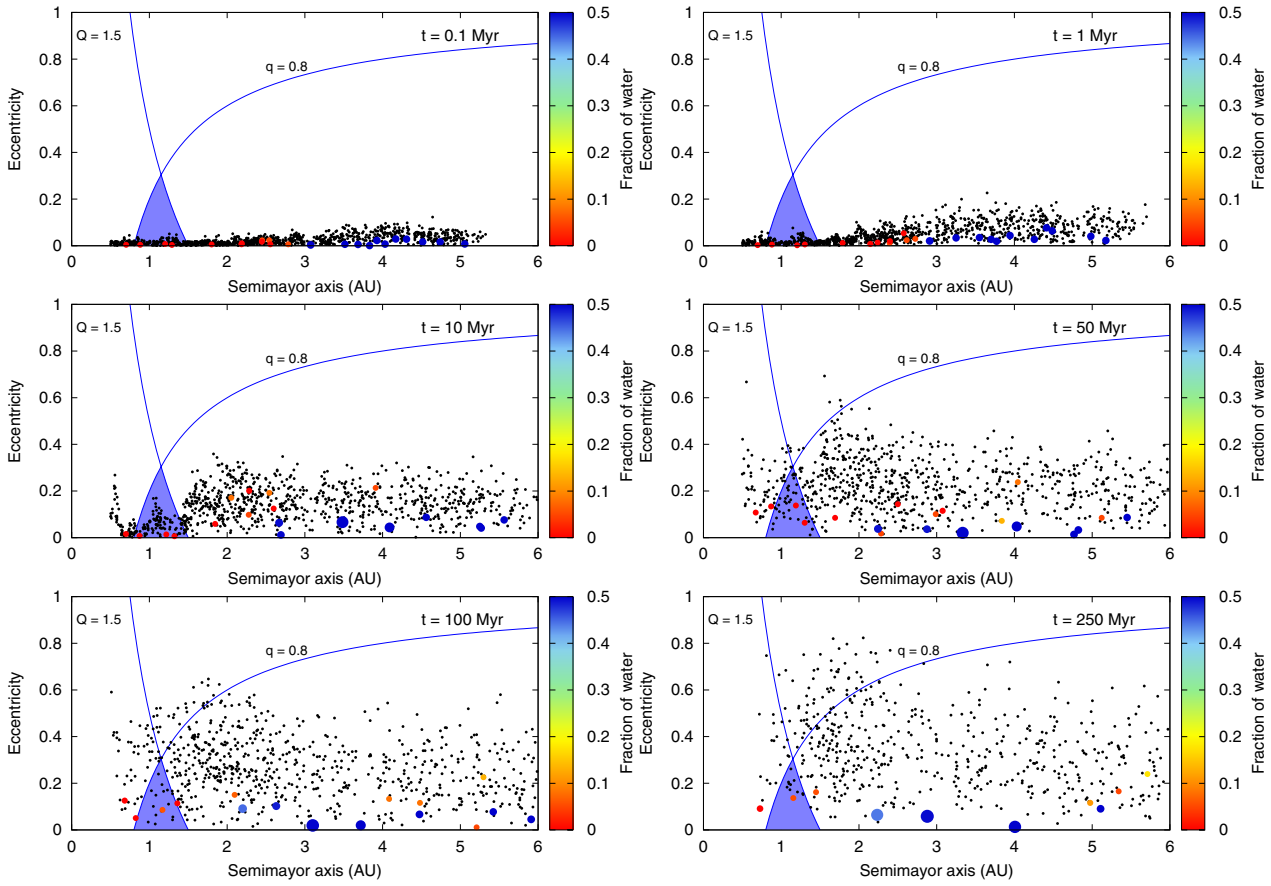

Fig. 1. Evolution in time of the S3 simulation for $\gamma = 0.5$. The light-blue shaded area represents the HZ and the curves with $q = 0.8$ AU and $Q = 1.5$ AU represent curves of constant perihelion and aphelion, respectively. Planetary embryos are plotted as colored circles and planetesimals are plotted with black dots. The color scale represents the fraction of water of the embryos relative to their masses. In this case there is only one embryo in the HZ, located at 1.15 AU with a mass of 0.03 $M_\oplus$ and a water content of 5.37% by mass, which represents six Earth oceans. The color figure is only available in the electronic version.

Table 1. General characteristics of the planets in the HZ for simulations S1, S2, and S3 for $\gamma = 0.5$.

Simulation	a_i (AU)	a_f (AU)	M ($M_\oplus$)	W (%)	T_{LGI} (Myr)
S1	0.95	0.94	0.1	4.44	146
S2	1.28	1.36	0.1	0.06	49
S3	1.20	1.15	0.03	5.37	–

Notes. a_i and a_f are the initial and the final semimayor-axis of the resulting planet in AU, M is the final mass in $M_\oplus$, W is the percentage of water by mass after 250 Myr, and T_{LGI} the timescale in Myr of the last giant impact. The planet in the HZ of S3 has not yet experienced a giant impact; it has only acreted planetesimals. As we mentioned in Sect. 4.1, this planet could collide with the third planet of the system if we had extended the simulations beyond 250 Myr.

All the simulations developed form planets in the HZ and one of the most important results to note is that none of them come from the outer zone of the disk, as we can see in Table 1. Since the surface density profile with $\gamma = 0.5$ is the least massive one in the inner zone of the disk, the gravitational interactions between bodies in this region are weak and there is no substantial mixing of solid material. Thus, embryos evolve very close to their initial positions and do not migrate from the outer zone to the inner zone. Because of this, they accrete most of the embryos and planetesimals from the inner zone than from the outer zone, beyond the snow line. This can be seen in Fig. 3, where the feeding zones of the planets that remain in the HZ of the S1, S2, and S3 simulations are plotted. The 91, 16% of the mass of planet a was originally situated before the snow line. Almost the total mass of planet b (99.9%) comes from the inner zone, and for planet c, 89.39% of the mass also comes from the zone inward of 2.7 AU.

All planets in the HZ present between 0.06% and 5.37% of water by mass. In particular, the planet in S1 with 0.1 $M_\oplus$ has ∼16 Earth oceans. The planet in S2 with a mass of 0.1 $M_\oplus$ presents ∼0.2 Earth oceans, and finally the planet in S3 with 0.03 $M_\oplus$ has ∼6 Earth oceans. Table 1 shows the general characteristics of the planets in the HZ for the three simulations S1, S2, and S3.

We highlight that planetesimals play an important role in these simulations because they are the part mainly responsible for the water content in the resulting planets. In fact, almost the total water content in the HZ planet for S1 is provided

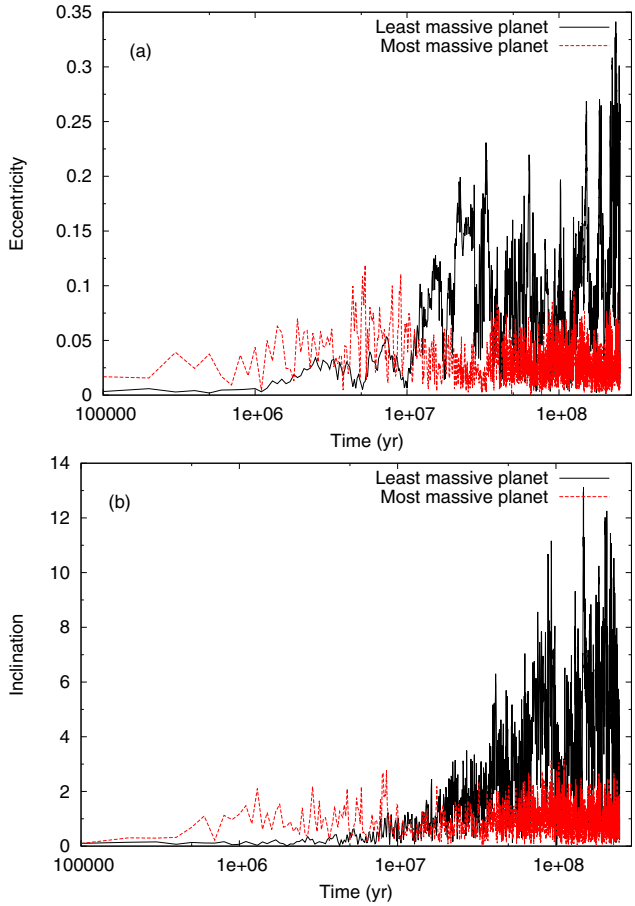

Fig. 2. Evolution in time of the eccentricities **a)** and inclinations **b)** for the least massive planet (black curve) and for the most massive planet (red dashed curve) of S3 simulation for $\gamma = 0.5$. The dynamical friction phenomena is evident for the most massive planet, which does not exceed values of eccentricity and inclination of 0.12 and 3.15°. In contrast, the least massive planet reaches highest values of eccentricity and inclination of 0.35 and 13°. The color figure is only available in the electronic version.

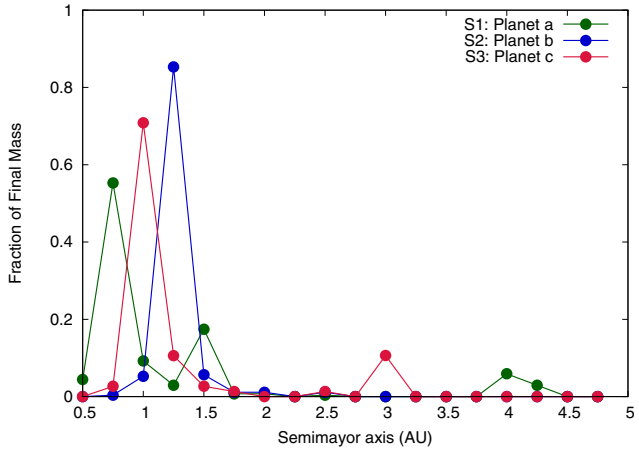

Fig. 3. Feeding zones of the planets that remain in the HZ of S1, S2, and S3 in disks with $\gamma = 0.5$. The y axis represents the fraction of each planet's final mass after 250 Myr. As can be seen, most of the mass acreted by these planets comes from the inner zone of the disk. The color figure is only available in the electronic version.

by planetesimals. However, planetesimals only provide 37.86% of the total mass, while the rest of the accreted mass is due to other embryo accretion. The same applies to the S2 and S3 simulations.

4.2. Simulations with $\gamma = 1$

We performed three simulations for 300 Myr. At that time, the planetesimals that still remained in the disk represent a small fraction of the original number, thus they will not modify the final results significantly. The final planetary systems present six or seven planets with a total mass ranging between 4 $M_\oplus$ and 4.45 $M_\oplus$, and the masses of individual planets is between 0.04 $M_\oplus$ and 1.9 $M_\oplus$. Here, all simulations present a planet in the HZ with a range of masses between 0.18 $M_\oplus$ and 0.52 $M_\oplus$ and with water contents from 2.54% to 9% of the total mass, which represents from 34 to 167 Earth oceans.

Figure 4 illustrates six snapshots in time of the semimayor-axis eccentricity plane of the evolution of the S3 simulation, which we consider to be the most representative for this density profile. The accretion process is similar to that described for the $\gamma = 0.5$ profile. At the end of the simulation the most important characteristics of the system can be described as follows: the system presents the innermost planet located at 0.73 AU, which has a mass of 0.36 $M_\oplus$, a planet located in the HZ with 0.37 $M_\oplus$, and the most massive planet placed at 2.54 AU with 1.26 $M_\oplus$. The rest of the simulations present similar results.

The dynamical friction effects are also relevant in this density profile from the beginning of the simulation and for the most massive bodies. Inclinations and eccentricities of the most massive bodies are damped by this dissipative force. Figure 5 shows the evolution in time of the eccentricities and inclinations of the most and least massive planet for the S3 simulation. The least massive planet reaches highest values of eccentricity and inclination of 0.64 and 31.53°, while the most massive planet does not exceed values of eccentricity and inclination of 0.14 and 6.48°. The difference with the same results for $\gamma = 0.5$ is that the scales of eccentricity and inclination are higher because this profile is more massive than the first one. All simulations for this profile show similar results for this phenomenon.

For the final number of resulting embryos and planetesimals, we obtain that ~6.2% of the planetesimals still survive in the study region after 300 Myr, while 20% of the embryos are still in the disk. These values represent 0.28 $M_\oplus$ and 4.46 $M_\oplus$ in planetesimals and embryos, respectively. Although there is still solid mass to continue the accretion process, this remaining mass in planetesimals only represents 3.53% of the initial mass in the study region. Therefore, it will not provide significant differences in the final planetary system. For this density profile the most important mass-removal mechanism remains the mass accretion because no embryo collides with the central star and none of them is ejected from the system. Of the mass in planetesimals, 16.4% collide with the central star and 11.5% are ejected from the disk. In this profile, in contrast to the previous one, the dynamical excitation is more evident since it is more massive in the inner zone of the disk, which provides a higher percentage of planetesimal ejections from the system and collisions with the central star.

As we reported above, one of the points of interest in this work is to study the planets that remain in the HZ. This profile also forms planets in the HZ and again, none of them come from the outer zone of the disk (see Table 2). Although this density profile with a value of $\gamma = 1$ presents more mass in the inner zone, it is still not enough to produce strong gravitational interaction between bodies, and therefore the mix of solid

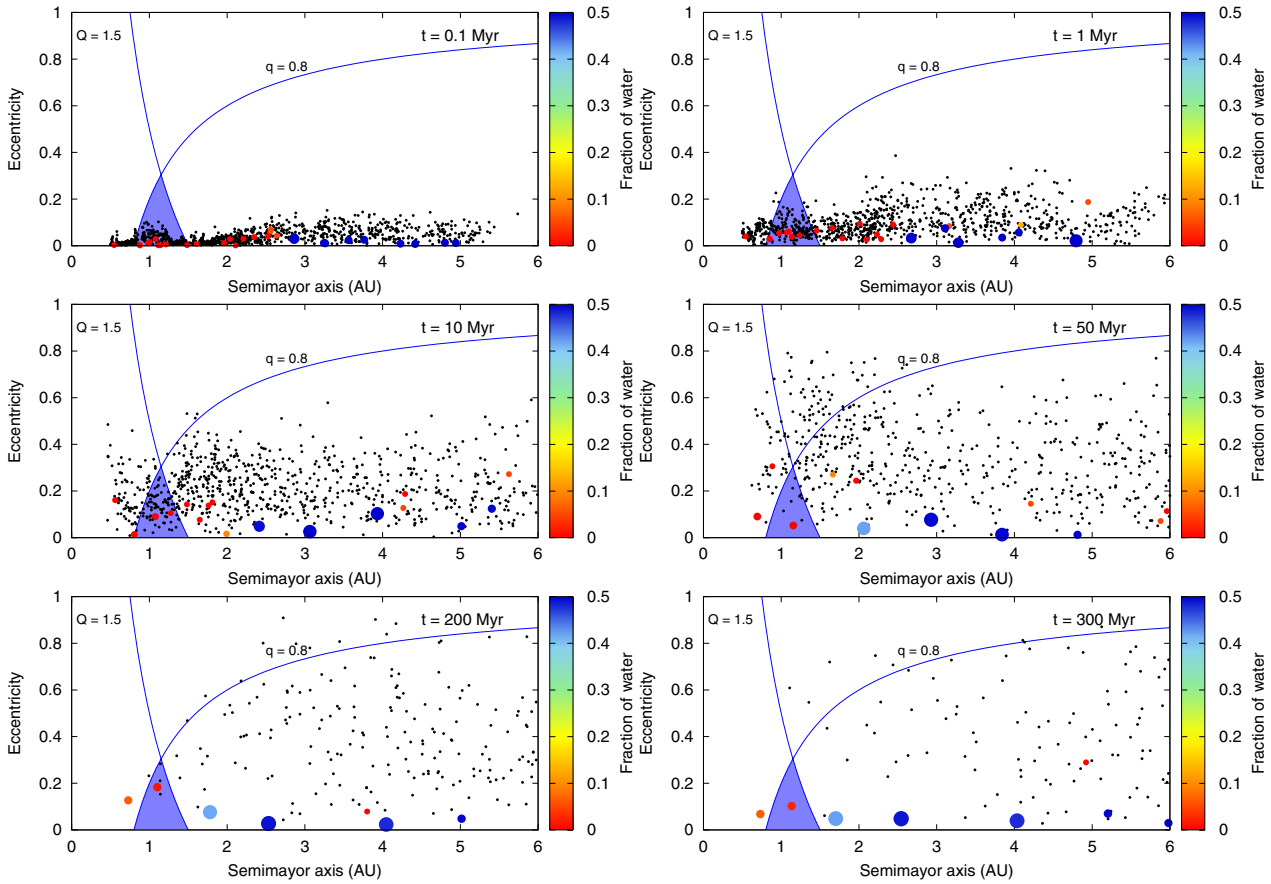

Fig. 4. Evolution in time of the S3 simulation for $\gamma = 1$. The light-blue shaded area represents the HZ and the curves with $q = 0.8$ AU and $Q = 1.5$ AU represent curves of constant perihelion and aphelion, respectively. Planetary embryos are plotted as colored circles, planetesimals with black dots. The color scale represents the fraction of water of the embryos relative to their masses. For this profile there is only one embryo in the HZ, located at 1.13 AU with a mass of $0.37 M_\oplus$ and a water content of 2.54% by mass, which represents 34 Earth oceans. The color figure is only available in the electronic version.

Table 2. General characteristics of the planets in the HZ for simulations S1, S2, and S3 for $\gamma = 1$.

Simulation	a_i (AU)	a_f (AU)	M ($M_\oplus$)	W (%)	T_{LGI} (Myr)
S1	0.84	0.83	0.52	9.00	110
S2	1.41	1.15	0.18	2.66	2
S3	0.99	1.02	0.37	2.54	78

Notes. a_i and a_f are the initial and the final semimayor-axis of the resulting planet in AU, M is the final mass in $M_\oplus$, W is the percentage of water by mass after 300 Myr, and T_{LGI} is the timescale in Myr of the last giant impact.

material is very low. Because of this, embryos evolve close to their initial positions and do not migrate from the outer to the inner zone. These planets accrete most of the embryos and planetesimals from the region inside the snow line. This can be seen in Fig. 6 where the feeding zones of the planets that remain in the HZ of the S1, S2, and S3 simulations are represented. In this case, 83.75% of the mass of planet a was originally situated inside 2.7 AU. 94.74% of the total mass of planet b come from the inner zone, and for planet c, 94.95% of the mass also come from the inner zone as well.

All planets resulting in the HZ for the three simulations present between 2.54% and 9% of water by mass. In particular, the planet in S1 with 0.52 $M_\oplus$ has ~167 Earth oceans. The planet in S2 with a mass of 0.18 $M_\oplus$ presents ~17 Earth oceans, the planet in S3 with 0.37 $M_\oplus$ has ~34 Earth oceans. Finally, Table 2 shows the general characteristics of the planets in the HZ for the three simulations S1, S2, and S3.

In general, all these planetary systems also show that the most responsible for the final water content are the planetesimals, which provide almost the total water content in the HZ planets. Nevertheless, they only provide between 30% to 50% of the final mass of the planet.

4.3. Simulations with $\gamma = 1.5$

Finally we describe the planetary systems with $\gamma = 1.5$. Because this is the most massive density profile in the inner zone of the disk, it is expected to be the most distinctive one, since the mass of the inner zone favors the formation of planets in the HZ.

We performed three different simulations and integrated them for 200 Myr. At the end of the simulations, there is almost no spare mass to continue the accretion process and thus, this result suggest that these systems have reached dynamical stability. The most relevant characteristics of the three simulations we

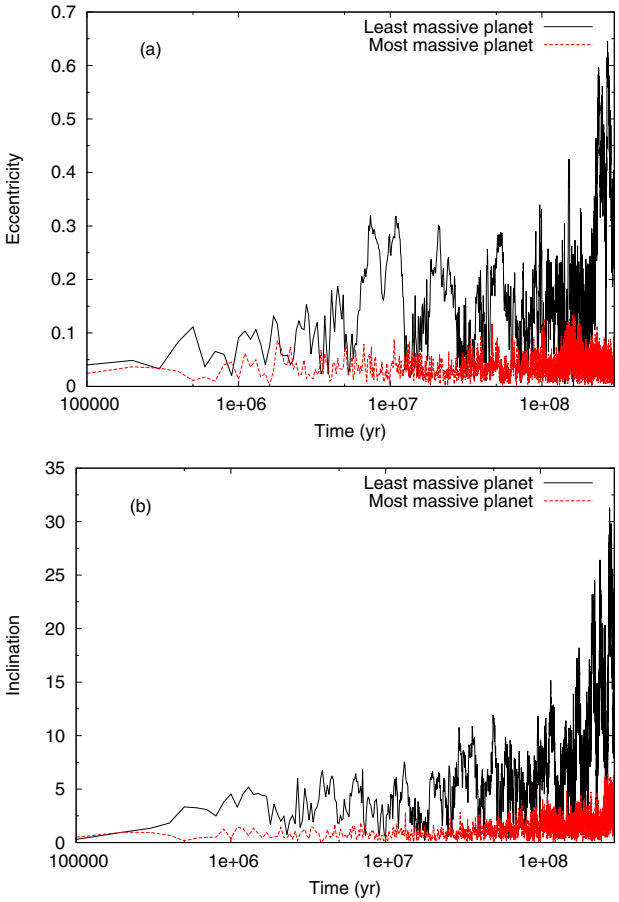

Fig. 5. Evolution in time of the eccentricities **a)** and inclinations **b)** for the least massive planet (black curve) and for the most massive planet (red dashed curve) of the S3 simulation for $\gamma = 1$. The dynamical friction phenomenon is evident for the most massive planet, which presents damped eccentricity and inclination. The scales of eccentricity and inclination are higher than the those in the first profile with $\gamma = 0.5$. The color figure is only available in the electronic version.

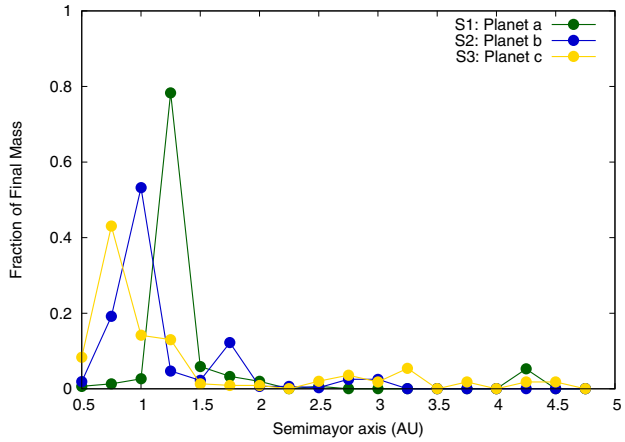

Fig. 6. Feeding zones of the planets that remain in the HZ of the S1, S2 and S3 in disks with $\gamma = 1$. The y axis represents the fraction of each planet's final mass after 300 Myr. Here again most of the mass acreted by these planets comes from the inner zone of the disk. The color figure is only available in the electronic version.

performed can be listed as follows: at the end of the simulations, the study region contains between four and seven planets with a total mass from 6.97 $M_\oplus$ to 8.81 $M_\oplus$. The mass of the final planets ranges between 0.06 $M_\oplus$ to 3.08 $M_\oplus$ and the resulting planets in the HZ present masses from 0.66 $M_\oplus$ to 2.21 $M_\oplus$. All simulations form a planet in the HZ, in particular, the S2 simulation forms two planets. We find that planets present ranges from 4.51% to 39.48% of water content in the HZ by mass, which represents from 192 to 2326 Earth oceans.

The S2 simulation is the most interesting one for this density profile because presents two planets in the HZ. This is why we chose this simulation for a more detailed description. Figure 7 shows six snapshots in time of the semimayor-axis eccentricity plane of the evolution of S2. In this case, the dynamical excitation of eccentricities and inclinations of both planetary embryos and planetesimals increases faster than in the other two described profiles. This promotes the mix of solid material between the inner and outer region of the snow line. After 200 Myr of evolution, the planetary system shows the innermost planet located at 0.47 AU with a mass of 0.60 $M_\oplus$, two planets in the HZ with 1.19 $M_\oplus$ and 1.65 $M_\oplus$ and the most massive planet placed at 3.35 AU, which has a mass of 2.15 $M_\oplus$.

This profile presents the most massive planets, which again shows the effects of dynamical friction. Indeed, the least massive planet of the S2 simulation reaches values of eccentricity and inclination of 0.79 and 48.56°, while the most massive planet presents highest values of eccentricity and inclination of 0.17 and 7.23°. This is illustrated in Fig. 8. Therefore, as shown, the tendency still holds that the effects of dynamical friction prevail over larger bodies. The main difference with the same results for the profiles with $\gamma = 0.5$ and $\gamma = 1$ is that the scales of eccentricities and inclinations are higher. All simulations for this surface density profile present similar results for this phenomena.

The S2 simulation ends with a 4.1% of survival planetesimals after 200 Myr between 0.5 AU and 5 AU, while 15.5% of the embryos are still in the disk. These values represent 0.43 $M_\oplus$ and 6.97 $M_\oplus$ in planetesimals and embryos, respectively. The remaining mass in planetesimals is not enough to modify the final planetary system significantly. Therefore the formation scales we used with this surface density profile are suitable. The most important mass-removal mechanism is, again, the mass accretion. No embryo collides with the central star, and none of them is ejected from the system. However, 23.4% of the planetesimals collide with the central star and 11.9% are ejected from the disk. This shows that the gravitational interactions between bodies are stronger than in the other profiles because the mass in the inner zone is larger than that associated with profiles with $\gamma = 0.5$ and 1.

All simulations present a planet in the HZ, one of them presents two. But this profile presents a distinctive and interesting characteristic that is different from the others. Two of the four planets that remain in the HZ come from the outer zone of the disk, this is, they come from beyond the snow line. This situation arises because of the solid material mix, which is stronger than in the other two profiles. As this profile is the most massive one in the inner zone, strong gravitational interactions are favored between bodies. This migration of the planets in the HZ for the S2 simulation can be seen in Table 3. This situation is also represented in Fig. 9 with the feeding zones of the planets that remain in the HZ of S1, S2, and S3. Here, only 35.98% of the mass of planet a was originally situated before 2.7 AU, the rest of the mass comes from the outer zone of the disk, beyond the snow line. Something similar occurs for planet c where only 25% of the mass comes from the inner zone. For planets b and d 90.98% and 83.79% of the total mass come from inside the snow line.

Finally, this seems to be the most peculiar profile because it presents *water worlds*, which are planets with high percentages of water contents by mass. All planets that remain in the HZ

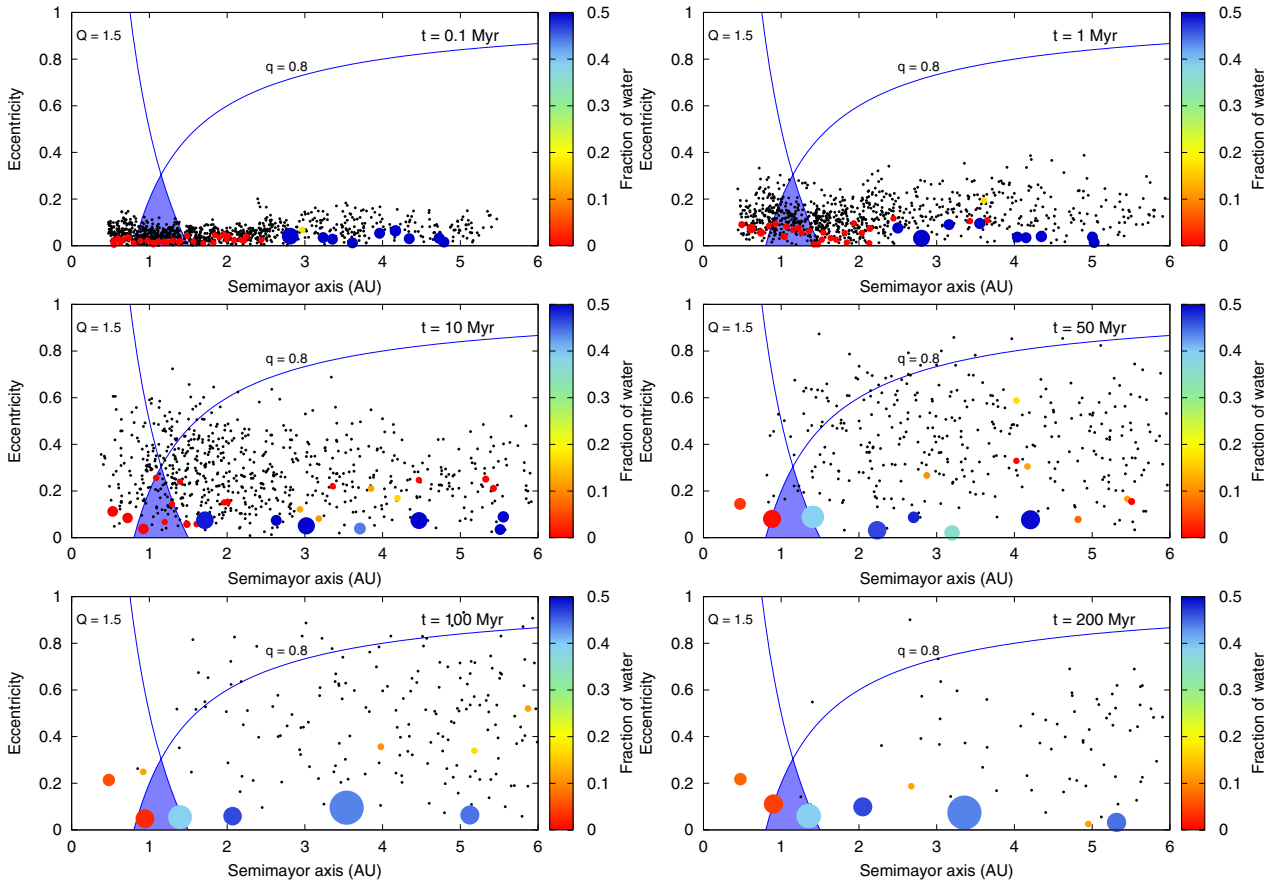

Fig. 7. Evolution in time of the S2 simulation for $\gamma = 1.5$. The light-blue shaded area represents the HZ and the curves with $q = 0.8$ AU and $Q = 1.5$ AU represent curves of constant perihelion and aphelion, respectively. Planetary embryos are plotted as colored circles, planetesimals with black dots. The color scale represents the fraction of water of the embryos with respect to their total masses. In this case there are two planets in the HZ with masses of 1.19 $M_\oplus$ and 1.65 $M_\oplus$. They present 4.51% and 39.48% of the water content by mass, which represents 192 and 2326 Earth oceans. The color figure is only available in the electronic version.

Table 3. General characteristics of the planets in the HZ for simulations S1, S2, and S3 for $\gamma = 1.5$.

Simulation	a_i (AU)	a_f (AU)	M ($M_\oplus$)	W (%)	T_{LGI} (Myr)
S1	4.52	1.41	2.21	32.55	32
S2	1.30	0.90	1.19	4.51	35
	3.13	1.35	1.65	39.48	22
S3	0.64	0.98	0.66	8.10	6

Notes. a_i and a_f are the initial and the final semimayor-axis of the resulting planet in AU, M is the final mass in $M_\oplus$, W is the percentage of water by mass after 200 Myr, and T_{LGI} is the timescale in Myr of the last giant impact.

for the three simulations present between 4.51% and 39.48% water content with respect to the total mass, being the embryos that come from beyond the snow line the ones that present larger amounts of water. In particular, the planet in S1 with 2.21 $M_\oplus$ has 32.55% water content, which represents ~2569 Earth oceans. This planet comes from the outer disk. The planets in the S2 simulation with masses of 1.19 $M_\oplus$ and 1.65 $M_\oplus$ present 4.51% and 39.48% water content, respectively, which is equal to 192 and 2326 Earth oceans, respectively. The first planet comes from the inner zone of the disk, the second one comes from the outer zone. In the S3 simulation, the planet in the HZ that comes from the inner zone of the disk has 0.66 $M_\oplus$ and shows 8.10% of water by mass, which represents ~191 Earth oceans. Lastly, Table 3 presents the general characteristics of the planets in the HZ for the three simulations S1, S2, and S3.

For the profiles with $\gamma = 0.5$ and $\gamma = 1$, planets in the HZ that do not come from beyond the snow line owe their water contents almost entirely to planetesimals, which are responsible for the ~50% of their final masses. However, the water content of the planets in the HZ that comes from the outer zone is almost entirely due to their initial water contents. Thus, for water worlds, planetesimals represent a secondary source of water.

5. Discussion and conclusions

We presented results for the formation of planetary systems without gaseous giants around Sun-like stars. In particular, our study assumed a low-mass protoplanetary disk with 0.03 $M_\odot$ and considered a wide range of surface density profiles. The choice

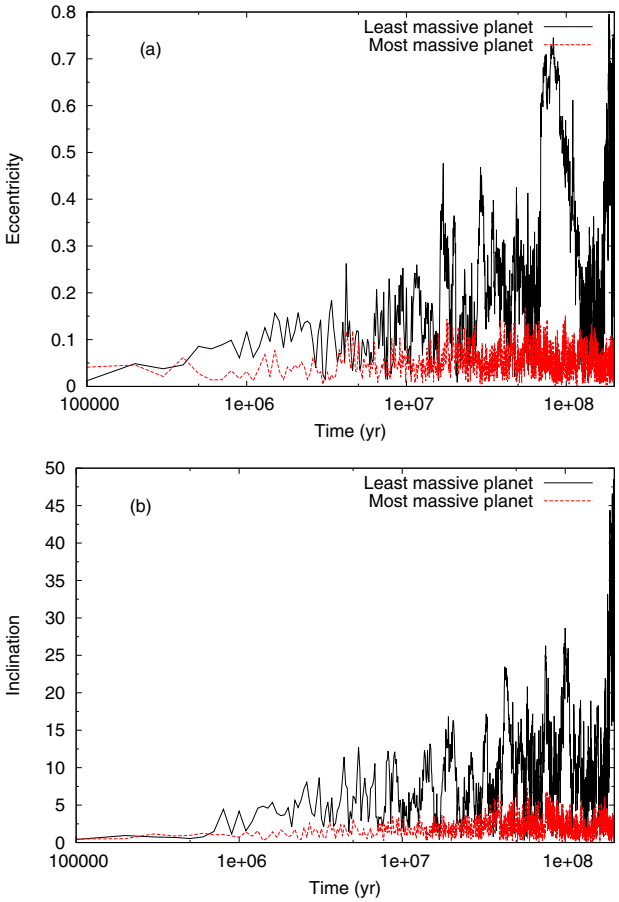

Fig. 8. Evolution in time of the eccentricities **a)** and inclinations **b)** for the least massive planet (black curve) and for the most massive planet (red dashed curve) of the S2 simulation for $\gamma = 1.5$. The dynamical friction phenomenon is evident for the most massive planet, which presents damped eccentricity and inclination. The scales of eccentricity and inclination are higher than those for $\gamma = 0.5$ and 1. The color figure is only available in the electronic version.

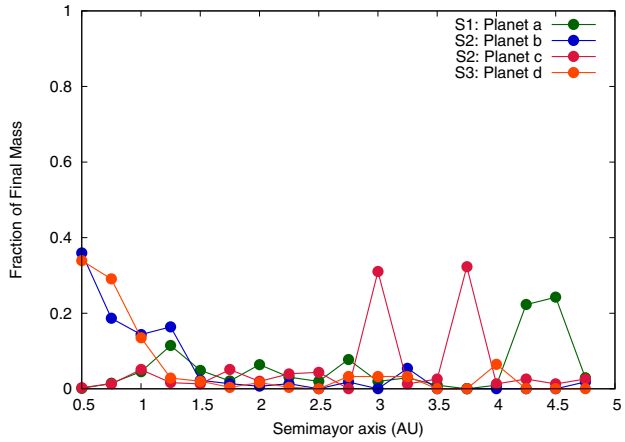

Fig. 9. Feeding zones of the planets that remain in the HZ of S1, S2, and S3 in disks with $\gamma = 1.5$. The y axis represents the fraction of each planet's final mass after 200 Myr. In this case, most of the mass acreted by planets b and d comes from the inner zone of the disk. But for planets a and c it is the other way arround. The color figure is only available in the electronic version.

of these conditions was based on results derived by Miguel et al. (2011), who suggested that a planetary system composed of only rocky planets is the most common outcome obtained from a low-mass disk (namely, $\lesssim 0.03\ M_\odot$) for different surface density profiles. We used a generic surface density profile characterized by a power law in the inner disk of the form $r^{-\gamma}$ and an exponential taper at large radii (Lynden-Bell & Pringle 1974; Hartmann et al. 1998). To describe a wide diversity of planetary systems, we chose values for γ of 0.5, 1, and 1.5. For each of these surface density profiles, we developed three N-body simulations of high resolution, which combined the interaction between planetary embryos and planetesimals. These N-body simulations allowed us to describe the dynamical evolution and the accretion history of each of the planetary systems of our study. In particular, these simulations analyzed the delivery of water to the resulting planets, allowing us to determine the importance of the systems under consideration from an astrobiological point of view.

The most interesting planets of our simulations are those formed in the HZ of the system. All the simulations formed planets in the HZ with different masses and final water contents depending on the surface density profile. Figure 10 shows the final configuration of all nine simulations. Here we can appreciate the diversity of possible planetary systems of terrestrial planets that might form around solar-type stars without giant gas planets and in low-mass disks.

For $\gamma = 0.5$, our simulations produced three planets in the HZ with masses ranging from 0.03 $M_\oplus$ to 0.1 $M_\oplus$ and water contents between 0.2 and 16 Earth oceans. While these planets are formed in the HZ and present final water contents similar to and even higher than that of the Earth, their masses do not seem to be large enough to retain a substantial and long-lived atmosphere, neither to sustain plate tectonics. In fact, Williams et al. (1997) proposed that the lower limit for habitable conditions is $M > 0.23\ M_\oplus$. Irrespective of the uncertainties in this value, we believe that such systems would not be of particular interest because the planets in the HZ would not be able to reach or overcome the estimated mass.

For $\gamma = 1$, three planets formed in the HZ with masses between 0.18 $M_\oplus$ and 0.52 $M_\oplus$ and water contents ranging from 34 to 167 Earth oceans. Although these final water contents represent upper limits, we inferred that the planets formed in the HZ from this surface density profile are water-rich bodies. On the other hand, their masses seem to be suitable considering the requirements for retaining a long-lived atmosphere and for maintaining plate tectonics (Williams et al. 1997). Thus, we suggest that the planets produced in the HZ from this surface density profile are of astrobiological interest.

For $\gamma = 1.5$, our simulations formed four planets in the HZ with masses ranging from 0.66 $M_\oplus$ to 2.21 $M_\oplus$ and water contents between 192 and 2326 Earth oceans. Taking into account the masses and the final water contents of these planets, these planetary systems are of special astrobiological interest. It is worth noting that this surface density profile shows distinctive results because it is the only one of those analyzed here that forms planets with very high proportion of water with respect to the composition of the entire planet. In fact, two of the planets formed in the HZ are water worlds with masses of 1.65 $M_\oplus$ and 2.21 $M_\oplus$ and 39.5 % and 32.6 % water by mass, respectively. For each of these cases, an embryo located beyond the snow line at the beginning of the simulation served as the accretion seed for the potentially habitable planet. It is very important to discuss the degree of interest of such water worlds from an astrobiological point of view. Abbot et al. (2012) studied the sensitivity of planetary weathering behavior and HZ to surface land fraction. They found that the weathering behavior is fairly insensitive to the land fraction for partially ocean-covered planets as long as the land fraction is greater than ~0.01. Thus, this

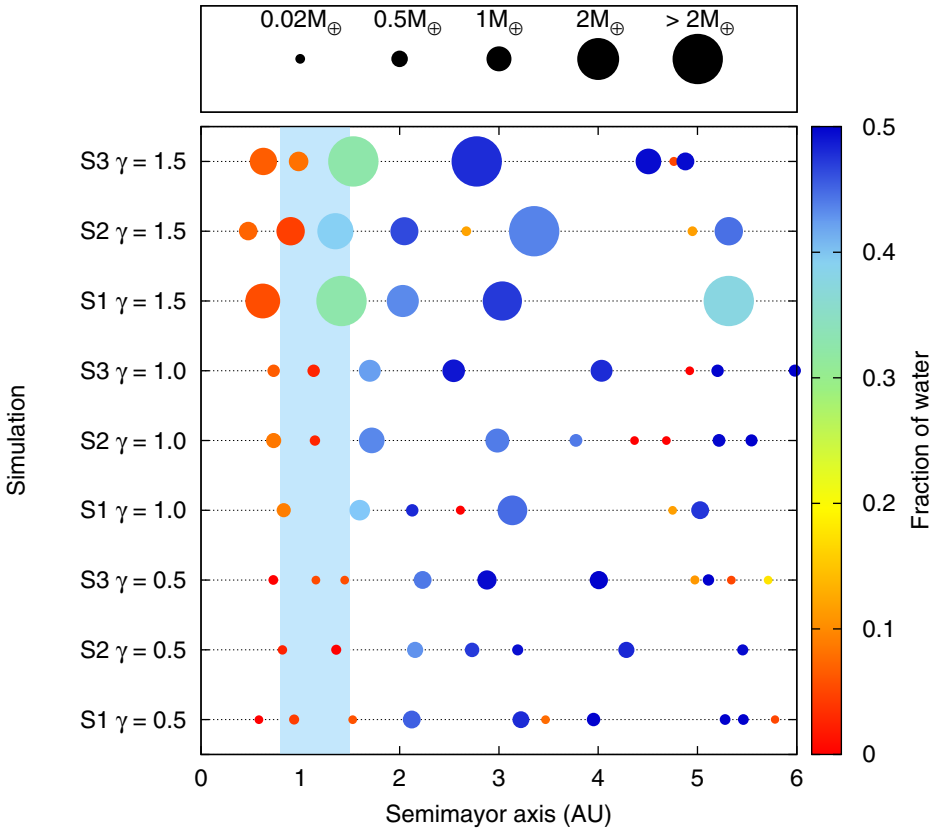

Fig. 10. Final configuration of all nine simulations. The color scale represents the water content of each planet, the shaded region represents the HZ between 0.8 AU and 1.5 AU. The size of each planet represents its relative physical size for the planets with masses lower than or equal to 2 $M_\oplus$.

Table 4. Initial and final amounts of solid mass in the HZ for each density profile.

γ	Initial mass in the HZ	Final mass in the HZ
0.5	0.104 $M_\oplus$	0.101 $M_\oplus$
1	0.605 $M_\oplus$	0.761 $M_\oplus$
1.5	1.423 $M_\oplus$	2.867 $M_\oplus$

study suggests that planets with partial ocean coverage should have a *habitable zone* of similar width. On the other hand, Abbot et al. (2012) also indicated that water worlds might have a much narrower *habitable zone* than a planet with even a small land fraction. Moreover, these authors suggested that a water world could "self-arrest" while undergoing a moist greenhouse from which the planet would be left with partial ocean coverage and a benign climate. The importance of surface and geologic effects on the water worlds is beyond the scope of this work. The water worlds represent a particular kind of exoplanets whose potential habitability needs to be studied in more detail.

The question remains whether the initial amount of mass in the HZ of the disk changes at the end of the simulations. Table 4 shows the initial and final amounts of solid mass in the HZ for each density profile. For $\gamma = 0.5$ and $\gamma = 1$ the values do not change significantly because the gravitational interactions between bodies in this region are weak and there is no substantial mixing of solid material. Thus, embryos evolve very close to their initial positions and the initial mass in the HZ remains basically the same. In contrast, the scenario is completely different for the third profile with $\gamma = 1.5$. Because this profile is the most massive one in the inner zone, strong gravitational interactions

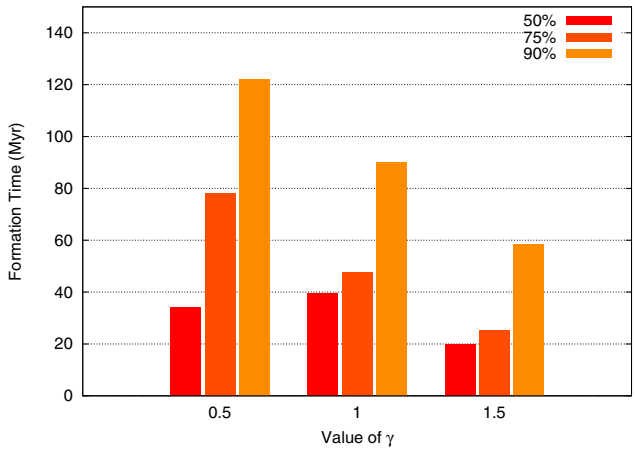

Fig. 11. Timescales for planets in the HZ to reach a given fraction (50%, 75%, or 90%) of their final masses, as a function of the surface density profile γ. These values are averages for all planets in the HZ of S1, S2 and S3 simulations.

are favored between bodies and some embryos migrate from the outer to the inner zone, adding mass in the HZ.

Figure 11 shows the mean time values that the planets need in the HZ to reach 50%, 75%, and 90% of their final mass for the three values of γ. Planets in the HZ for $\gamma = 0.5$ form more slowly than those in the HZ for $\gamma = 1$ and $\gamma = 1.5$. Since this profile is the least massive in the inner zone of the disk, the gravitational interactions between bodies are week. Thus, the accretion timescales for planets are longer than for the other profiles.

We can describe two scenarios within our simulations for the water delivery. Less massive disks in the inner zone, like those

with $\gamma = 0.5$ and $\gamma = 1$, form six planets in the HZ with water contents ranging from 0.03% to 9% by mass. On the other hand, disks with $\gamma = 1.5$, which are more massive, form four planets in the HZ with water contents ranging from 4.51% to 39.48% by mass. In the first scenario planetesimals are mainly responsible for this water content, while in the second scenario we find planets in which planetesimals are responsibles for their water content and planets in which embryos play the principal role. In fact, for $\gamma = 1.5$, for two of the planets in the HZ that come from beyond the snow line, the embryos are the responsibles of their water content, and for the other two planets that come from the inner zone of the disk, the planetesimals are mainly responsible for their final water content. Morbidelli et al. (2000) showed that the bulk of the Earth water was accreted by a few asteroidal embryos from beyond 2–2.5 AU, while Raymond et al. (2007a) proposed that terrestrial planets accrete a similar amount of water in the form of a few water-rich embryos and millions of planetesimals. However, the simulations of Raymond et al. (2007a) showed that the fraction of water delivered by planetesimals is much larger than that delivered by embryos[4]. Although the architecture of our planetary systems is very different from that studied by Morbidelli et al. (2000) and Raymond et al. (2007a) because we did not consider the existence of giant gaseous planets, the results of the first scenario of our simulations present the same trend as those of Raymond et al. (2007a). Nevertheless, when the mass of the inner part of the disk increases, we find that some of our results are consistent with those of Morbidelli et al. (2000) and some are consistent with those of Raymond et al. (2007a).

Raymond et al. (2005) analyzed the terrestrial planet formation in disks with varying surface density profiles. To do this, they considered that the surface density varies as $r^{-\gamma}$, and assumed three different values for γ: 0.5, 1.5, and 2.5. We emphasize that these authors did not take into account an increase in surface density due to the condensation of water beyond the snow line. On the other hand, Raymond et al. (2005) considered a fixed mass of material equal to 10 $M_\oplus$ between 0.5 AU and 5 AU for each distribution, and assumed that the disk mass is dominated by embryos, that have swept up the mass in their corresponding feeding zones. Finally, these authors developed the simulations including a Jupiter-mass giant planet at 5.5 AU. In this scenario, the individual masses of the planetary embryos in the outer region of the system are larger for lower values of γ. The larger the mass of the embryos in the outer region, the more significant the scattering of water-rich material in the entire system. For this reason, Raymond et al. (2005) found a more efficient water delivery for $\gamma = 0.5$ than for $\gamma = 1.5$.

In our simulations, we assumed surface density distributions of the form $r^{-\gamma}$ and explored three different values for γ of 0.5, 1, and 1.5. Unlike Raymond et al. (2005), we assumed a disk with a fixed mass of 0.03 $M_\odot$, which leads to a total mass of solids between 0.5 AU and 5 AU of 3.21 $M_\oplus$, 7.92 $M_\oplus$, and 13.66 $M_\oplus$, for $\gamma = 0.5$, 1, and 1.5, respectively. In our work the individual masses of the planetary embryos in the outer region of the system are therefore larger for higher values of γ. Accordingly, the distribution with $\gamma = 1.5$ leads to a more significant scattering of water-rich material that is associated with the outer region of the system. For this reason, our results suggest that the water delivery is more efficient for $\gamma = 1.5$ than for $\gamma = 0.5$. Our results are consistent with those obtained by Raymond et al. (2005) because in both studies the water delivery is more efficient in systems that contain the most massive embryos in the outer region.

To determine the final water content of the resulting planets of our simulations, we adopted an initial distribution of water content that was based on data for primitive meteorites from Abe et al. (2000). We analyzed the sensitivity of our results to the initial distribution of water assumed for the protoplanetary disk. To do this, we considered a simple prescription for assigning initial water contents to embryos and planetesimals as a function of their radial distances. We assumed that bodies inside 2.7 AU do not have water, while bodies beyond 2.7 AU contain 50% water by mass. From this new initial distribution, we did not find relevant changes in the final water contents of the resulting planets of our simulations. This result confirms that the water delivery to the planets located at the HZ is provided primarily by embryos and planetesimals that started the simulation beyond the snow line. The initial water content of the bodies located inside the snow line does not lead to relevant changes in our results.

By analyzing the masses and water contents of the planets formed in the HZ of our simulations, we concluded that the surface density profiles with $\gamma = 1$ and 1.5 produce planetary systems of special astrobiological interest from a low-mass disk. It is therefore very interesting to discuss if planets analogous to those formed in the HZ of such systems can be discovered with the current detection techniques. The NASA *Kepler* mission[5] was developed with the main purpose of detecting Earth-size planets in the HZ of solar-like stars (Koch et al. 2010). To date, this mission has discovered 167 confirmed planets and over 3538 unconfirmed planet candidates. The Kepler-37 system hosts the smallest planet yet found around a star similar to our Sun (Barclay et al. 2013a). This planet, which is called Kepler-37b, is significantly smaller than Mercury and is the innermost of the three planets of the system at 0.1 AU. On the other hand, the smallest HZ planets discovered to date by the *Kepler* mission are Kepler-62e, 62f (Borucki et al. 2013) and 69c (Barclay et al. 2013b) with 1.61, 1.41, and 1.71 Earth radii, respectively. The potentially habitable planets formed in all our simulations have sizes ranging from 0.38 to 1.6 Earth radii, assuming physical densities of 3 g cm^{-3}. Thus, the *Kepler* mission would seem to be able to detect the potentially habitable planets of our simulations very soon. However, in May 2013, the *Kepler* spacecraft lost the second of four gyroscope-like reaction wheels, which ended new data collection for the original mission. Currently, the *Kepler* mission has assumed a new concept, dubbed K2, to continue with the search for other worlds. A decision about it is expected by the end of 2013. Future missions, such as PLAnetary Transits and Oscillations of stars (PLATO 2.0; Rauer 2013), will play a significant role in the detection and characterization of terrestrial planets in the *habitable zone* around solar-like stars during the next decade. In fact, the primary goal of PLATO is to assemble the first catalogue of confirmed planets in *habitable zones* with known mean densities, compositions, and evolutionary stages. This mission will play a key role in determining how common worlds like ours are in the Universe, and also how suitable they are for the development and maintenance of life.

In addition to the detection of planets in the HZ, we can ask whether it is possible to distinguish the planetary systems of interest obtained in our simulations. The gravitational microlensing technique will probably play a significant role in

[4] A comparison between Morbidelli et al. (2000), Raymond et al. (2007a) and this work needs to be made with care since the scenarios and their treatments are quite different, mainly because our scenario does not include a giant planet.

[5] http://kepler.nasa.gov/

the detection of planetary systems similar to those obtained in our work. Unlike other techniques, such as the transit method or radial velocities, the microlensing technique is sensitive to planets on wide orbits around the snow line of the system (Gaudi 2012). Currently, the main microlensing surveys for exoplanets are the Optical Gravitational Lensing Experiment (OGLE; Udalski 2003) and the Microlensing Observations in Astrophysics (MOA; Sako et al. 2008). To date, a total number of 26 planets have been detected by these surveys. The least massive planets discovered to date by the microlensing technique are MOA-2007-BLG-192-L b (Bennett et al. 2008) and OGLE-05-390L b (Beaulieu et al. 2006), with $3.3^{+4.9}_{-1.6}$ $M_\oplus$ and $5.5^{+5.5}_{-2.7}$ $M_\oplus$, respectively. MOA-2007-BLG-192-L b and OGLE-05-390L b orbit stars with $0.06^{+0.028}_{-0.021}$ $M_\odot$ and $0.22^{+0.21}_{-0.11}$ $M_\odot$, respectively. The lowest-mass exoplanet found to date orbiting a Sun-like star is OGLE-2012-BLG-0026L b (Han et al. 2013). This planet is located at ∼3.8 AU from the central star and has 0.11 ± 0.02 M_J, where M_J represents a Jupiter mass.

The planets formed in our simulations that might be found by the microlensing technique are significantly less massive than those detected to date by these techniques. For $\gamma = 0.5$, our simulations formed planets of ∼0.5 $M_\oplus$ between 2.1 AU and 4.3 AU. For $\gamma = 1$, the resulting system shows planets with masses ranging from 1.4 $M_\oplus$ to 1.9 $M_\oplus$ between 1.7 AU and 3.2 AU. Finally, for $\gamma = 1.5$, our simulations produced planets with masses of 2.2 $M_\oplus$ to 3.1 $M_\oplus$ between 2.7 AU and 3.4 AU. Again, the current microlensing surveys have not yet detected planets analogous to those formed on wide orbits in our simulations. However, future surveys such as the Korean Microlensing Telescope Network (KMTNet; Poteet et al. 2012) and the Wide-Field InfraRed Survey Telescope (WFIRST; Green et al. 2011) will play an important role in the search of exoplanets by the microlensing technique. KMTNet is a ground-based project with plans to start operations in 2015. WFIRST is a space-based project that is scheduled for launch in 2020. In particular, the main goal of WFIRST is to detect via microlensing planets with masses $\gtrsim$0.1 $M_\oplus$ and separations $\gtrsim$0.5 AU, including free-floating planets. Therefore, planetary systems similar to those formed in the present work will probably be detected by microlensing techniques within this decade.

The main result of this study suggests that the planetary systems without gas giants that harbor 1.4–3.1 $M_\oplus$ planets on wide orbits around Sun-like stars are very interesting from an astrobiological point of view. This work complements that developed by de Elía et al. (2013), which indicated that systems without gas giants that harbor super-Earths or Neptune-mass planets on wide orbits around solar-type stars are of astrobiological interest. These theoretical works offer a relevant contribution for current and future observational surveys because they allow us to determine which planetary systems are of special interest.

Acknowledgements. We are grateful to Pablo J. Santamaría, who provided us with the numerical tools necessary to study the collisional history and water accretion in planets in the H.Z. and thank Juan P. Calderón, who kindly helped us to improve the plots of the time evolution of all our simulations. Finally we thank the referee, Sean Raymond, for valuable suggestions, which helped us to improve the manuscript.

References

Abbot, D. S., Cowan, N. B., & Ciesla, F. J. 2012, ApJ, 756, 178
Abe, Y., Ohtani, E., Okuchi, T., Righter, K., & Drake, M. 2000, in Water in the Early Earth, eds. R. M. Canup, K. Righter, et al., 413
Andrews, S. M., Wilner, D. J., Hughes, A. M., Qi, C., & Dullemond, C. P. 2009, ApJ, 700, 1502
Andrews, S. M., Wilner, D. J., Hughes, A. M., Qi, C., & Dullemond, C. P. 2010, ApJ, 723, 1241
Barclay, T., Burke, C. J., Howell, S. B., et al. 2013a, ApJ, 768, 101
Barclay, T., Rowe, J. F., Lissauer, J. J., et al. 2013b, Nature, 494, 452
Beaulieu, J.-P., Bennett, D. P., Fouqué, P., et al. 2006, Nature, 439, 437
Bennett, D. P., Bond, I. A., Udalski, A., et al. 2008, ApJ, 684, 663
Borucki, W. J., Agol, E., Fressin, F., et al. 2013, Science, 340, 587
Chambers, J. E. 1999, MNRAS, 304, 793
Chambers, J. E., & Cassen, P. 2002, Meteoritics, 37, 1523
Chiang, E., & Laughlin, G. 2013, MNRAS, 431, 3444
Cumming, A., Butler, R. P., Marcy, G. W., et al. 2008, PASP, 120, 531
Dauphas, N., & Pourmand, A. 2011, Nature, 473, 489
Davis, S. S. 2005, ApJ, 627, L153
de Elía, G. C., Guilera, O. M., & Brunini, A. 2013, A&A, 557, A42
Desch, S. J. 2007, ApJ, 671, 878
Dullemond, C. P., Hollenbach, D., Kamp, I., & D'Alessio, P. 2007, in Protostars and Planets V, eds. B. Reipurth, D. Jewitt, & K. Keil (Tucson: University of Arizona Press), 555
Garaud, P., & Lin, D. N. C. 2007, ApJ, 654, 606
Gaudi, B. S. 2012, ARA&A, 50, 411
Green, J., Schechter, P., Baltay, C., et al. 2011, unpublished [arXiv:1108.1374]
Han, C., Udalski, A., Choi, J.-Y., et al. 2013, ApJ, 762, L28
Hartmann, L., Calvet, N., Gullbring, E., & D'Alessio, P. 1998, ApJ, 495, 385
Hayashi, C. 1981, Prog. Theor. Phys. Suppl., 70, 35
Kasting, J. F., Whitmire, D. P., & Reynolds, R. T. 1993, Icarus, 101, 108
Koch, D. G., Borucki, W. J., Basri, G., et al. 2010, ApJ, 713, L79
Kokubo, E., & Ida, S. 1998, Icarus, 131, 171
Kokubo, E., Kominami, J., & Ida, S. 2006, ApJ, 642, 1131
Kuchner, M. J. 2004, ApJ, 612, 1147
Lécuyer, C., & Gillet, P., & Robert, F. 1998, Chem. Geol., 145, 249
Lodders, K. 2003, ApJ, 591, 1220
Lynden-Bell, D., & Pringle, J. E. 1974, MNRAS, 168, 603
Mandell, A. M., Raymond, S. N., & Sigurdsson, S. 2007, ApJ, 660, 823
Marty, B. 2012, Earth Planet. Sci. Lett., 313, 56
Mayor, M., & Queloz, D. 2012, New Astron. Rev., 56, 19
Miguel, Y., Guilera, O. M., & Brunini, A. 2011, MNRAS, 417, 314
Morbidelli, A., Chambers, J., Lunine, J. I., et al. 2000, Meteoritics, 35, 1309
Mordasini, C., Alibert, Y., Benz, W., & Naef, D. 2009, A&A, 501, 1161
Poteet, W. M., Cauthen, H. K., Kappler, N., et al. 2012, in SPIE Conf. Ser., 8444
Rauer, H. 2013, European Planetary Science Congress 2013, held 8-13 September in London, UK
Raymond, S. N., & Cossou, C. 2014, MNRAS, 440, L11
Raymond, S. N., Quinn, T., & Lunine, J. I. 2004, Icarus, 168, 1
Raymond, S. N., Quinn, T., & Lunine, J. I. 2005, ApJ, 632, 670
Raymond, S. N., Quinn, T., & Lunine, J. I. 2006, Icarus, 183, 265
Raymond, S. N., Quinn, T., & Lunine, J. I. 2007a, Astrobiology, 7, 66
Raymond, S. N., Scalo, J., & Meadows, V. S. 2007b, ApJ, 669, 606
Raymond, S. N., O'Brien, D. P., Morbidelli, A., & Kaib, N. A. 2009, Icarus, 203, 644
Sako, T., Sekiguchi, T., Sasaki, M., et al. 2008, Exp. Astron., 22, 51
Selsis, F., Kasting, J. F., Levrard, B., et al. 2007, A&A, 476, 1373
Touboul, M., Kleine, T., Bourdon, B., Palme, H., & Wieler, R. 2007, Nature, 450, 1206
Tsiganis, K., Gomes, R., Morbidelli, A., & Levison, H. F. 2005, Nature, 435, 459
Udalski, A. 2003, Acta Astron., 53, 291
Ward, W. R. 1997, Icarus, 126, 261
Weidenschilling, S. J. 1977, Ap&SS, 51, 153
Williams, D. M., Kasting, J. F., & Wade, R. A. 1997, Nature, 385, 234